MIT Libraries | DSpace@MIT

MIT Open Access Articles

The effect of velocity uncertainty on migrated reflectors: Improvements from relative-depth imaging

The MIT Faculty has made this article openly available. ***Please share*** how this access benefits you. Your story matters.

Citation: Poliannikov, Oleg V., and Alison E. Malcolm. "The Effect of Velocity Uncertainty on Migrated Reflectors: Improvements from Relative-Depth Imaging." GEOPHYSICS 81, no. 1 (November 6, 2015): S21–S29. © 2015 Society of Exploration Geophysicists

As Published: http://dx.doi.org/10.1190/GEO2014-0604.1

Publisher: Society of Exploration Geophysicists

Persistent URL: http://hdl.handle.net/1721.1/100940

Version: Final published version: final published article, as it appeared in a journal, conference proceedings, or other formally published context

Terms of Use: Article is made available in accordance with the publisher's policy and may be subject to US copyright law. Please refer to the publisher's site for terms of use.

Massachusetts Institute of Technology

GEOPHYSICS, VOL. 81, NO. 1 (JANUARY-FEBRUARY 2016); P. S21–S29, 7 FIGS.
10.1190/GEO2014-0604.1

Downloaded 01/12/16 to 18.51.1.3. Redistribution subject to SEG license or copyright; see Terms of Use at http://library.seg.org/

The effect of velocity uncertainty on migrated reflectors: Improvements from relative-depth imaging

Oleg V. Poliannikov[1] and Alison E. Malcolm[2]

ABSTRACT

We have studied the problem of uncertainty quantification for migrated images. A traditional migrated image contains deterministic reconstructions of subsurface structures. However, input parameters used in migration, such as reflection data and a velocity model, are inherently uncertain. This uncertainty is carried through to the migrated images. We have used Bayesian analysis to quantify the uncertainty of the migrated structures by constructing a joint statistical distribution of the location of these structures. From this distribution, we could deduce the uncertainty in any quantity derived from these structures. We have developed the proposed framework using a simple model with velocity uncertainty in the overburden, and we estimated the absolute positions of the horizons and the relative depth of one horizon with respect to another. By quantifying the difference in the corresponding uncertainties, we found that, in this case, the relative depths of the structures could be estimated much better than their absolute depths. This analysis justifies redatuming below an uncertain overburden for the purposes of the uncertainty reduction.

INTRODUCTION

Seismic depth migration is a general process by which seismic events in recorded data are moved from time to depth coordinates (Yilmaz, 2001). This process traditionally produces a single deterministic image with no uncertainty description. Any subsequent interpretation is based on this image as if it were an accurate representation of the subsurface. To go from data recorded in time to an image that represents the subsurface in depth, any implementation of depth migration requires a velocity model. This velocity model is obtained from prior surveys and analysis, and it is assumed to be given for the purpose of migration. Obtaining an accurate velocity model in practice is a nontrivial problem, and the final velocity model is an approximation of the true velocity model that can be associated with some uncertainty. This uncertainty propagates to the migrated image as a whole and to the locations of individual horizons in particular (Grubb et al., 2001; Bube et al., 2004a, 2004b; Kane et al., 2004; Pon and Lines, 2005; Glogovsky et al., 2009; Osypov et al., 2011).

A natural question is, what information contained in the image can we believe? Does the uncertainty in the input parameters affect all horizons found in the migrated image in the same way? It is clear that the estimated depth of any given structure becomes uncertain if the migration velocity is uncertain. It has been shown (e.g., Fomel and Landa, 2014) that an incorrect velocity may also lead to structural deformations in the image, but the continuity of imaged horizons is nonetheless more stable than their positions if the velocity perturbations are relatively smooth. This shows that some of the spatial information contained in the image is more reliable than other information. Proper uncertainty quantification is necessary to understand what information in the image is reliable and what is not.

A naïve way to quantify uncertainty in a seismic image is to describe a joint probability distribution of all its grid points. For a 3D survey, this would result in a distribution with many millions or even billions of variables. Conceptually, this distribution would contain all existing statistical information about the image. However, this approach is not only impractical due to the exorbitant requirements of computational resources and memory but it is also most probably useless. Assuming such an object could be constructed, it is not obvious how we can use it in a meaningful way. Analysis of seismic data primarily aims to extract useful information from the volume of the recorded data in a compact and manageable form; it is rarely useful to further inflate this already very large data volume.

Manuscript received by the Editor 21 December 2014; revised manuscript received 29 July 2015; published online 6 November 2015.
[1]Massachusetts Institute of Technology, Department of Earth, Atmospheric and Planetary Sciences, Earth Resources Laboratory, Cambridge, Massachusetts, USA. E-mail: poliann@mit.edu.
[2]Memorial University of Newfoundland, Department of Earth Sciences, St. John's, Newfoundland, Canada. E-mail: amalcolm@mun.ca.
© 2015 Society of Exploration Geophysicists. All rights reserved.

Downloaded 01/12/16 to 18.51.1.3. Redistribution subject to SEG license or copyright; see Terms of Use at http://library.seg.org/

In this paper, we regard continuous events in the recorded data as basic objects that can be considered in the data or, after migration, in the model space. For the purposes of uncertainty quantification, we approximate all events at discrete points with small line segments in 2D or small planar patches in 3D. The original horizon could then be reconstructed from these linear patches by interpolation. We then use map migration/demigration (Douma and de Hoop, 2006) in a given velocity to transform these line segments (or patches) between the data space and the model space. We use it on one or several horizons simultaneously to study how they jointly migrate and demigrate in different velocity models. Map migration/demigration provides a fast, tractable, physical model that can be used as a basis for statistical uncertainty quantification. As with any approximate method, map migration may not be suitable for constructing images in some cases, even in the noise-free scenario with a known velocity model. Although we would not be able to recover quantitative uncertainties in these cases, following the map-migration procedure outlined here would give at least some idea of the uncertainties, and particularly of how the uncertainties in different horizons are related to one another.

The Bayesian uncertainty analysis that we advocate in this paper recovers the absolute and relative positions of seismic horizons along with their associated uncertainties. It follows a similar analysis of location uncertainty for seismic events (Poliannikov et al., 2013, 2014). Given surface seismic reflection data, we construct a joint posterior estimator of the locations of chosen horizons that is a multidimensional probability distribution of the locations of discrete points on the horizons. This probability distribution describes the likelihood of each horizon location and the correlation between possible locations of different horizons. It is derived from a prior probability of the horizon locations, which can be uninformed, and a likelihood function that describes the probability of observing a particular data set given fixed horizon locations.

Our analysis shows that in some cases, the location of one structure relative to another can be estimated with much smaller uncertainty than the absolute depth of individual structures, and this difference in the uncertainties of absolute locations and relative locations can be exactly quantified. This analysis is applicable in many situations from redatuming below a complicated near surface to updating a model during monitoring while drilling. The uncertainty in the image constructed using surface data includes velocity uncertainty throughout the volume. However, having drilled to a certain depth, we know the model up to that depth and we may be interested only in the part of the model that lies below. Absolute depths of deeper horizons can then be inferred from the current absolute depth of the drill bit and the relative depths of these horizons. If the uncertainty in the relative imaging is smaller than the uncertainty in the absolute imaging, then a better image of the subsurface can be constructed than the one initially obtained from the surface data.

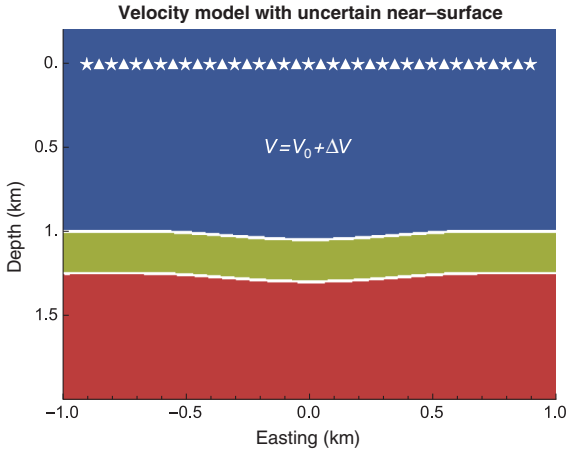

Figure 1. A numerical acoustic model with a background velocity of 2 km/s, two reflectors, and sources and receivers at the surface. The part of the medium above the first reflector ($z = 1$ km) is uncertain in later examples. The velocity below the reflector $z \geq 1$ is assumed to be known.

THEORY

Problem setup and velocity uncertainty

We first consider a simple acoustic model with two embedded reflectors to illustrate our framework; we extend this model to more complicated situations below. Sources and receivers are located on the surface as shown in Figure 1. The velocity model is uncertain. We model the velocity uncertainty by assuming that the velocity V belongs to a family of admissible velocity models $\mathcal{V}$. The probability distribution $p(V)$ determines the likelihood of any velocity model from the family $\mathcal{V}$.

Proper identification of a suitable velocity distribution $p(V)$ is very important because the results of the uncertainty analysis will follow from the assumptions we make about possible sources of uncertainty. In some cases, $p(V)$ may be defined analytically; however, it does not have to be. Most crucial in applications is the ability to sample from the probability distribution $p(V)$, i.e., to generate multiple realizations of plausible velocity models so that their effect on migration can be explicitly considered. In practice, these plausible velocity models may come from different sources, some of which we discuss below.

Extrapolated blocked sonic logs may be used as approximations for migration velocity models. The amplitude of velocity fluctuations in the log around the chosen value for any given depth may be viewed as a measure of velocity uncertainty. When the velocity model is estimated using tomographic methods, an a priori defined cost functional may be minimized using numerical optimization. When the convergence condition is satisfied, it is typically assumed that the correct velocity model has been found. However, it is conceptually possible to let the optimization algorithm continue to run and explore other velocity models that are all consistent with the data used in the inversion. Thus, we would naturally obtain samples of plausible velocity models. If the velocity is obtained using some type of moveout analysis, then the size of the spot defined by high semblance values (or something similar) could also be a good measure of velocity uncertainty.

Figure 2 shows the result of the velocity analysis for the numerical model shown in Figure 1 using shots and receivers with offsets up to ± 1.5 km and normalized velocity stacking. In this case, we could infer that velocity uncertainty could be as high as 5%–10%, up to 200 m/s. If we used a different array or if the reflectors had a different geometry, the velocity uncertainty would be different. For the purpose of our discussion, the exact methodology used to quantify the velocity uncertainty is not important. We assume that the velocity analysis has been performed and thus the family of admissible velocities $\mathcal{V}$ and the probability distribution $p(V)$ have been

Downloaded 01/12/16 to 18.51.1.3. Redistribution subject to SEG license or copyright; see Terms of Use at http://library.seg.org/

identified, and we proceed to describe the experiment and the problem of quantifying the uncertainty of reflector positions.

We fire a shot at each source location (Figure 1) and record a corresponding common-shot gather. These common-shot gathers are resorted, for example, to common-offset gathers, and individual reflections are picked in the sorted gathers. The problem is to describe the location and shape of the reflectors along with the associated uncertainties from the reflected events in the gathers. The current discussion relies on the picking of event traveltimes in common-offset gathers and migrates those picked times directly. This is, of course, not ideal for a real data set. In that case, we would expand our data in a suitable basis, e.g., curvelets (Douma and de Hoop, 2007) or similar, and we migrate the time indices of these bases' functions. This is a subject of current work.

Map migration

For a 2D survey in a 3D space, each event in a common-offset gather can be approximated with a collection of 5-tuple as follows:

$$(x_d, y_d, t_d, p_d^x, p_d^y), \tag{1}$$

where x_d, y_d are common-midpoint coordinates, t_d is the traveltime, and

$$p_d^x = \frac{1}{2}\frac{\partial t_d}{\partial x_d}, \qquad p_d^y = \frac{1}{2}\frac{\partial t_d}{\partial y_d} \tag{2}$$

are the horizontal slownesses of the unmigrated reflection.

For simplicity, we will work in 2D, where $y_d \equiv 0$ and $p_d^y \equiv 0$, and the event in the data domain has the form $(x_d, t_d, p_d \equiv p_d^x)$. All results, however, generalize directly to 3D (Douma and de Hoop, 2006). For a homogeneous isotropic medium with velocity V, the traveltime is governed by the double-square-root equation as follows:

$$t_d = \frac{1}{V}\sqrt{(x_d - x_m - h)^2 + \left(\frac{Vt_m}{2}\right)^2} + \frac{1}{V}\sqrt{(x_d - x_m + h)^2 + \left(\frac{Vt_m}{2}\right)^2}. \tag{3}$$

Here x_m is the coordinate of the reflection point, h is the half-offset, z_m is the depth, $t_m = 2z_m/V$ is the two-way migrated traveltime, and we define

$$p_m = \frac{1}{2}\frac{\partial t_m}{\partial x_m} = \frac{1}{V}\frac{\partial z_m}{\partial x_m}. \tag{4}$$

Douma and de Hoop (2006) derive an analytic formula for the coordinates of the migrated reflector embedded in the known velocity model (x_m, z_m, p_m) from the specular reflection coordinates (x_d, t_d, p_d). They also present a 3D version of this formula that could be used to extend our results to 3D. This relationship, which we will denote by $\mathcal{M}$, has the following form:

$$\begin{aligned} x_m &= x_d - \left(\frac{Vt_d}{2}\right)^2 \frac{\Lambda_d}{h}, \\ z_m &= V\left(\frac{t_d^2}{4} - \frac{h^2}{V^2} + \left(\frac{Vt_d\Lambda_d}{4h}\right)^2\left(\frac{4h^2}{V^2} - t_d^2\right)\right)^2, \\ p_m &= \frac{1}{2}p_d t_d |\Lambda_d - 1||\Lambda_d + 1| \\ &\quad \times \left(\frac{t_d^2}{4} - \frac{h^2}{V^2} + \left(\frac{Vt_d\Lambda_d}{4h}\right)^2\left(\frac{4h^2}{V^2} - t_d^2\right)\right)^{-\frac{1}{2}}, \end{aligned} \tag{5}$$

where

$$\Lambda_d = \frac{1}{2\sqrt{2}p_d h}\sqrt{\Theta_d\left(1 - \sqrt{1 - \frac{64(p_d h)^4}{\Theta_d^2}}\right)} \tag{6}$$

and

$$\Theta_d = t_d^2 + \left(\frac{2h}{V}\right)^4 \frac{1}{t_d^2} - 2\left(\frac{2h}{V}\right)^2 (1 - (Vp_d)^2). \tag{7}$$

The demigration equations describe the transformation $\mathcal{D}$ back from (x_m, z_m, p_m) to (x_d, t_d, p_d) (Douma and de Hoop, 2006):

$$\begin{aligned} x_d &= x_m + Vp_m z_m + h\Lambda_m, \\ t_d &= \sqrt{\frac{4h^2}{V^2} + \frac{4p_m h z_m}{V\Lambda_m}}, \\ p_d &= \frac{p_m 2z_m}{V|\Lambda_m - 1||\Lambda_m + 1|\sqrt{\frac{4h^2}{V^2} + \frac{4p_m h z_m}{V\Lambda_m}}}, \end{aligned} \tag{8}$$

where

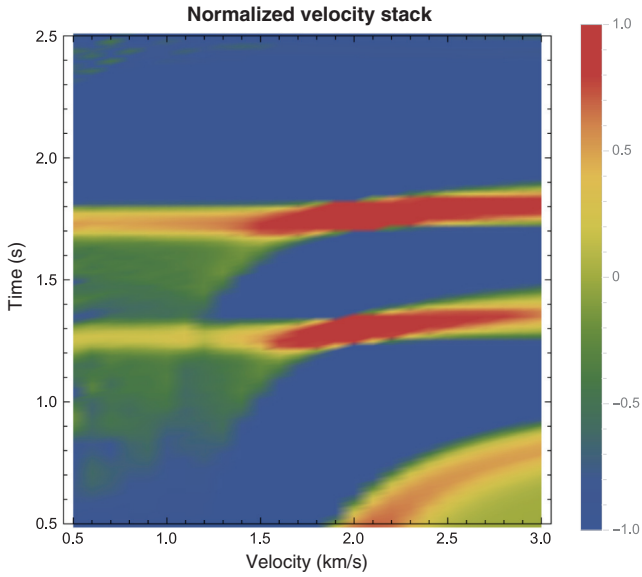

Figure 2. Result of velocity analysis performed for the model shown in Figure 1 using shots and receivers with offsets up to ±1.5 km. The source central frequency is 10 Hz.

$$\Lambda_m = \frac{4p_m h}{\Theta_m\left(1+\sqrt{1+\frac{16(p_m h)^2}{\Theta_m^2}}\right)} \tag{9}$$

with

$$\Theta_m = \frac{2z_m}{V}(1+V^2p_m^2). \tag{10}$$

Migrating horizons from the data domain into the model domain and demigrating them in the opposite direction using map migration/demigration are therefore very straightforward and extremely fast. The regularized versions of these formulas obtained by Taylor approximations could be used for small offsets or short times to ensure numerical stability. This allows us to do inversion with Bayesian uncertainty quantification in a computationally efficient way.

Bayesian uncertainty analysis

Forward model

If the velocity V is known, and there is no noise in the data, then any infinitesimal reflector can be represented in the model domain as a pair $\ell_m \equiv (x_m, z_m, p_m)$, where (x_m, z_m) is the location the reflector and p_m is the half-slope, or in the data domain as a triplet $\ell_d \equiv (x_d, t_d, p_d)$. These two representations are related through the operators of map migration $\mathcal{M}$ and map demigration $\mathcal{D}$:

$$(x_d, t_d, p_d) \equiv \ell_d \overset{\mathcal{M}}{\rightarrow} \ell_m \equiv (x_m, z_m, p_m), \tag{11}$$

and

$$(x_m, z_m, p_m) \equiv \ell_m \overset{\mathcal{D}}{\rightarrow} \ell_d \equiv (x_d, t_d, p_d). \tag{12}$$

In practice, the velocity model is never known exactly and the recorded data are noisy. Velocity randomness and the noise in the recordings introduce a random component in the reflection-time data, and the problem becomes that of recovering the model of the subsurface from these observations. We solve this problem by Bayesian inversion. The Bayesian framework is based on the notion of the likelihood function. Consider a model that consists of a set of reflectors $\ell_m \equiv (x_m, z_m, p_m)$, an assumed model V, and the half-offset h. Here and throughout the remainder of the paper, we always understand that we deal with a collection of triplets. The observed data are then written as

$$\hat{t}_d = t_d + n_t, \tag{13}$$

where

$$(x_d, t_d, p_d) = \mathcal{D}(x_m, z_m, p_m | V, h), \tag{14}$$

and we explicitly indicate the velocity V and half-offset h used in the demigration operator. We assume that there is no noise in the x_d component, i.e., $\hat{x}_d = x_d$, because the traveltimes are registered at fixed receiver locations. The noise n_t is assumed to be a realization of a zero-mean Gaussian process with some correlation length l in a horizontal position. If reflection times were picked independently at each receiver, the correlation length would be zero: $l = 0$. However, because in practice events are picked in the entire gather, the pick in any given trace depends on the signal content at neighboring traces, and the correlation length may be greater than zero: $l > 0$. We estimate the noisy slownesses $\hat{p}_d$ from $\hat{t}_d$ by a second-order finite-difference approximation.

Inversion in the known velocity with fixed offset

We denote the likelihood function that describes possible observed data and their probabilities as $p(\hat{\ell}_d \mid \ell_m, h, V)$ and the prior as $p(\ell_m)$. Applying Bayes' formula yields the following inversion:

$$p(\ell_m \mid \hat{\ell}_d, h, V) \propto p(\hat{\ell}_d \mid \ell_m, h, V)p(\ell_m). \tag{15}$$

Equation 15 provides an exact expression for the posterior distribution of the model parameters. However, if each reflector is approximated relatively finely, then the total number of model parameters is very large. To simplify the computation and the representation of the posterior distribution of the horizon locations, we approximate our collection of reflectors with a multivariate Gaussian distribution:

$$(x_m, z_m) \sim \mathcal{N}((x_m^0, z_m^0), \Sigma^0), \tag{16}$$

where (x_m, z_m) denotes all of the reflectors approximating the horizon.

Following standard Gaussian analysis, the mean of this multinormal distribution is found by maximizing the previously defined likelihood function:

$$(x_m^0, z_m^0) = \underset{x_m, z_m, p_m = \frac{1}{2}\frac{\partial z_m}{\partial x_m}}{\arg\max}\, p(\hat{x}_d, \hat{t}_d, \hat{p}_d \mid x_m, z_m, p_m, h, V)p(x_m, z_m, p_m) \tag{17}$$

subject to the constraints

$$\hat{x}_d = x_d, \quad \hat{p}_d = \frac{1}{2}\frac{\partial \hat{t}_d}{\partial x_d}. \tag{18}$$

Effectively, we search for reflectors in the model space that best explain the observed data. The uncertainty around these maximum-likelihood positions is assumed Gaussian with the covariance matrix given by the inverse Hessian of the logarithm of the function inside the arg max in equation 17 at its maximum point.

Inversion in uncertain velocity from multioffset data

Equations 15 and 16 provide expressions for migrated reflector coordinates in a known velocity V model for a fixed half-offset h. Forward-model predicted data in multiple common-offset gathers $\hat{\ell}_d \equiv (\hat{x}_d, \hat{t}_d, \hat{p}_d)$ can be obtained by combining data predicted for every available offset as described above. In general, a model (x_m, z_m, p_m) is now evaluated as likely if it fits the observed data across different offsets after a demigration with a plausible velocity model. Formally, when the velocity is uncertain, we integrate the product of the likelihood function and the prior to obtain the velocity independent posterior.

More specifically, we denote the reflectors in the model domain $\ell_m \equiv (x_m, z_m, p_m)$, the combined observed reflection data sorted in

Downloaded 01/12/16 to 18.51.1.3. Redistribution subject to SEG license or copyright; see Terms of Use at http://library.seg.org/

Downloaded 01/12/16 to 18.51.1.3. Redistribution subject to SEG license or copyright; see Terms of Use at http://library.seg.org/

all common-offset gathers $\hat{\ell}_d \equiv (\hat{x}_d, \hat{t}_d, \hat{p}_d)$, and the velocity V. We have from Bayes' formula that

$$p(\ell_m, V \mid \hat{\ell}_d) = \frac{p(\hat{\ell}_d \mid \ell_m, V)p(\ell_m, V)}{p(\hat{\ell}_d)}, \tag{19}$$

where

$$p(\hat{\ell}_d) = \iint p(\hat{\ell}_d \mid \ell_m, V)p(\ell_m, V)d\ell_m dV. \tag{20}$$

A velocity-independent description of the uncertainty in the reflector positions ℓ_m can be obtained from the joint (ℓ_m, V) posterior by integrating over the velocity variable:

$$\begin{aligned} p(\ell_m \mid \hat{\ell}_d) &= \int p(\ell_m, V \mid \hat{\ell}_d)d \\ &= \int \frac{p(\hat{\ell}_d \mid \ell_m, V)p(\ell_m, V)}{p(\hat{\ell}_d)} dV \\ &= \frac{1}{p(\hat{\ell}_d)} \int p(\hat{\ell}_d \mid \ell_m, V)p(\ell_m)p(V)dV \\ &= \frac{1}{p(\hat{\ell}_d)} \mathsf{E}_V[p(\hat{\ell}_d \mid \ell_m, V)p(\ell_m)], \end{aligned} \tag{21}$$

where E_V denotes the expected value over admissible velocity models. Thus, we can write the following equation:

$$p(\ell_m \mid \hat{\ell}_d) \propto \mathsf{E}_V[p(\hat{\ell}_d \mid \ell_m, V)p(\ell_m)]. \tag{22}$$

The formal expectation, E_V in equation 22 can be approximated with a mean over a sample from the velocity distribution. If the family of admissible velocities $\mathcal{V}$ is large and multidimensional, then producing a large number of sample velocities from this distribution to assure the convergence of the average to the theoretical mean may be a nontrivial problem. Several methods to speed up Bayesian inversion have been proposed in the literature (Tierney, 1994). Discussing them in more detail is beyond the scope of this paper. In the examples in the next section, we will look at a simple illustration for the proposed methodology, in which the numerical computation of the expectation over different velocity models V is easy.

NUMERICAL EXAMPLES

Two reflectors in a layered medium

We illustrate the proposed methodology with simple numerical examples. The model is as described above with sources and receivers at the surface and two reflectors in the subsurface (Figure 1). The velocity in the overburden is uncertain, and the recorded data are assumed to be noisy. The noise in the signal would lead to erroneous picking of the specular reflection events. We model picked traveltimes by ray tracing the model and adding Gaussian correlated noise to resulting arrival times. Most picking algorithms enforce some kind of continuity of a horizon that will lead to correlation between picking errors at nearby traces. The correlation length of the picking error process is taken to be $l = 1$ km in the horizontal position, and the standard deviation of the signal noise in each trace

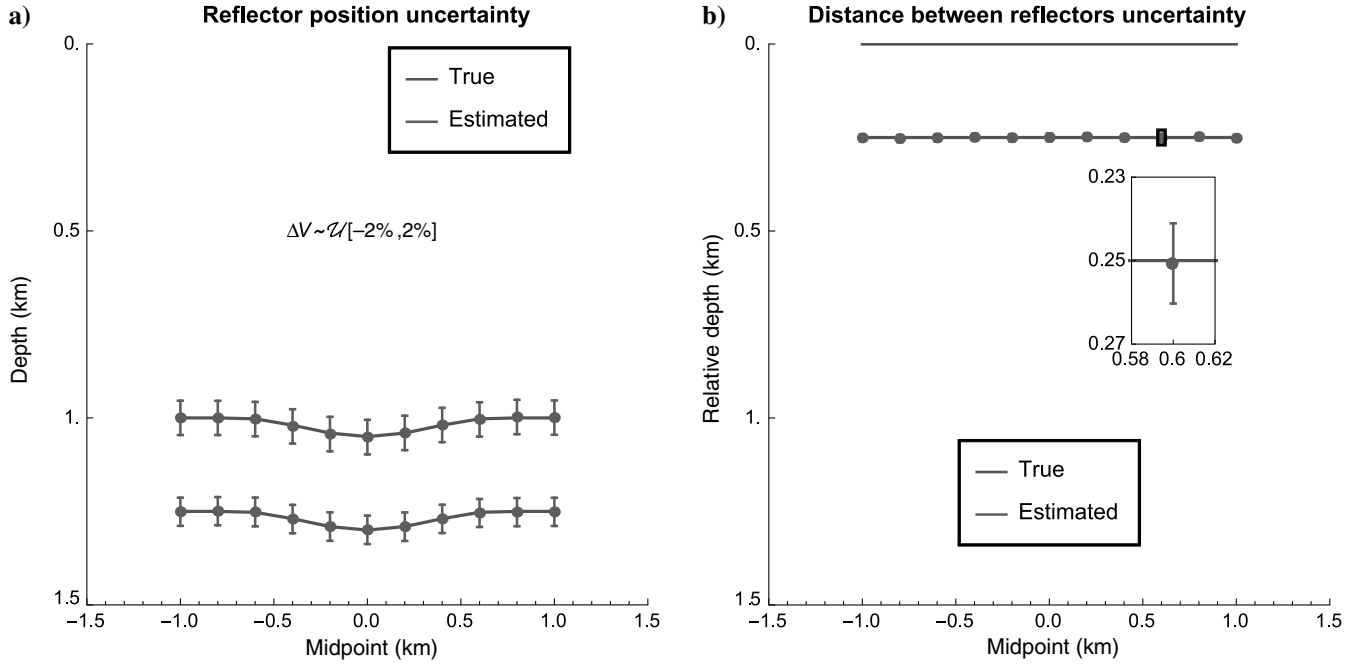

Figure 3. (a) Variations in the position of the migrated reflectors when the overburden velocity is uncertain: $V = V_0 + \Delta V$, where $\Delta V \sim \mathcal{U}[-2\%, 2\%]$. The lines denote the true reflector positions, and the error bars show the three-standard-deviation region plotted with vertical exaggeration to show the reflector shape. (b) The relative depth of the second reflector with respect to the depth of the first one. The inset shows one of the error bars magnified. The effect of the velocity uncertainty is much smaller for the relative depth than for each depth individually.

Downloaded 01/12/16 to 18.51.1.3. Redistribution subject to SEG license or copyright; see Terms of Use at http://library.seg.org/

is 1 ms. We now consider two cases of velocity uncertainty. In both cases, the velocity above the reflectors is uncertain, and the velocity below the first reflector is presumed known. We model velocity uncertainty by assuming that the velocity in the overburden is uniformly distributed between two values, which are shown for each numerical experiment. This is a simplistic model for a geology frequently encountered in the Middle East, in which karsts and dunes sit on top of a layered cake of slowly varying sediments. For each numerical setup, we compute the posterior given by equation 22 by approximating the expectation with an average over velocity samples. The number of velocity samples is such that the convergence of the average to the theoretical expectation is detected.

Precision of relative imaging

In the first example shown in Figure 3, the velocity estimate in the "overburden" has an uncertainty of $\pm 2\%$. We compute the posterior distribution for both reflectors with equation 22. In Figure 3a, we plot the true positions of each reflector. We also compute the offset-dependent means μ and standard deviations σ of the depth of each reflector, and we indicate the boundaries of the $\mu \pm 3\sigma$ intervals with error bars. In Figure 3b, we show the relative depth of the second reflector with respect to the depth of the first reflector. The vertical axes of the two panels have the same scale, so that the error bars in the absolute and relative depth domains can be directly compared.

Estimators for the absolute and relative depths do not exhibit any noticeable bias because of the geometry of the horizons and the unbiased uncertainty in the velocity. However, a comparison of the panels reveals a marked reduction in uncertainty in relative depth compared with the absolute depth. The relative depth reconstruction is more stable in this example because much of the velocity uncertainty, in the overburden, has little effect on the relative depth. The relative depth primarily depends on the difference of the reflection times from the two reflectors. This traveltime difference is not significantly affected by the velocity variations in the overburden if the scale of the velocity perturbations in the overburden is sufficiently large because for each source-receiver pair, reflected waves travel through nearby parts of the layered overburden. For small velocity variations, different reflection times may not reduce uncertainty to the same extent or even at all. By appropriately choosing a family of admissible velocity models $\mathcal{V}$, we can calculate precisely what uncertainty reduction, if any, is to be expected from using relative imaging.

Accuracy of relative imaging

In the second example shown in Figure 4, we assume that the prior velocity is biased. More specifically, we let the velocity in the overburden above the first reflector be overestimated by a random error that is distributed uniformly between 0% and 5%. The velocity between the reflectors is still assumed to be known. As before, Figure 4a contains the results of the uncertainty analysis of the absolute depths of the migrated reflectors.

The absolute depths of both reflectors are underestimated due to the fast velocities used for migration. At the same time, the relative depth of the second reflector with respect to the depth of the first reflector is once again recovered much better. No bias in the estimate of the relative depth is present due to the cancellation of the effect of the velocity error, and this estimate is much more precise.

Before moving to a more complicated model, we show one more test in Figure 5, in which we underestimate the velocity by 2%–5%. This example is particularly interesting because all assumed velocity realizations are wrong, whereas previously, the correct velocity model ($\Delta V = 0\%$) was part of the assumed family of admissible

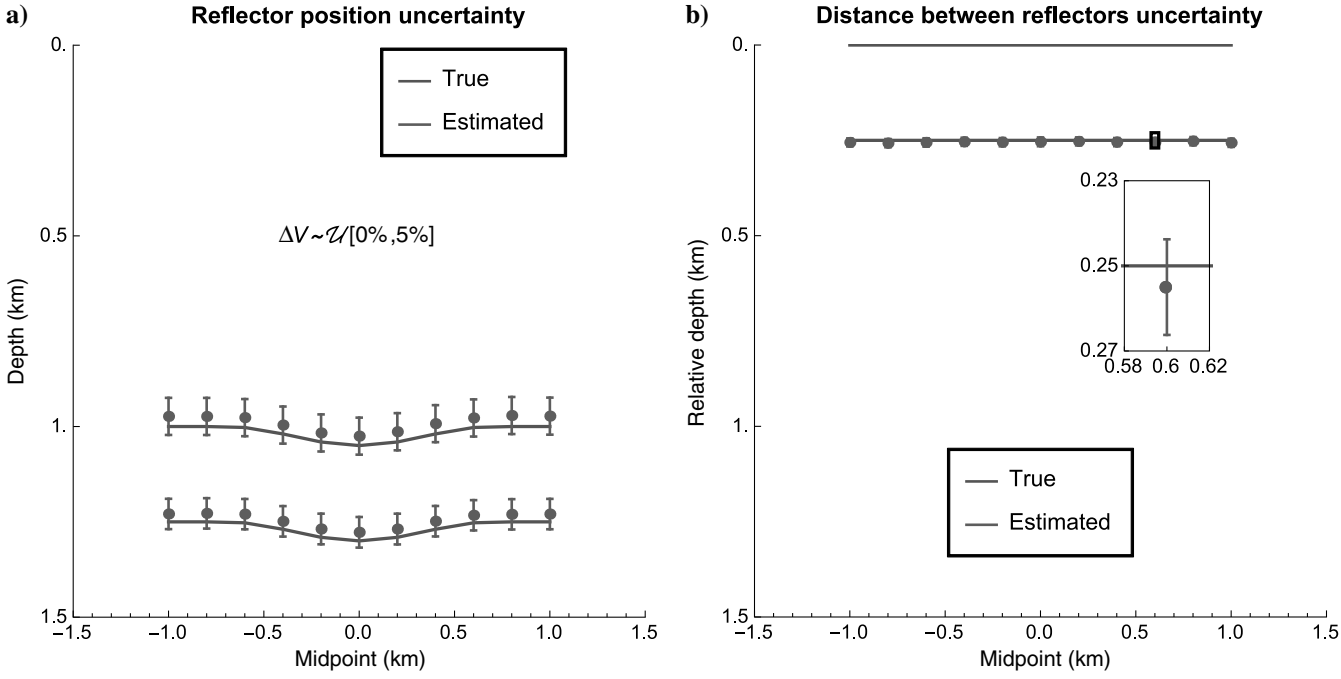

Figure 4. (a and b) Same as Figure 3 but with $\Delta V \sim \mathcal{U}[0\%, 5\%]$. Note that the error bars have a similar size, but they are now biased because the estimated velocities range from correct to too fast; however, we do not include any that are too slow.

Downloaded 01/12/16 to 18.51.1.3. Redistribution subject to SEG license or copyright; see Terms of Use at http://library.seg.org/

velocities $\mathcal{V}$. When the correct velocity is not included, the forward model may be, strictly speaking, incompatible with the data. Because the analysis presented above uses the forward model, its results may be misleading if our assumptions about the velocity uncertainty, signal noise, etc., are not satisfied.

Two reflectors in a model with a lens

In the second example shown in Figure 6, a homogeneous velocity model contains a fast inclusion. The velocity increase inside the inclusion relative to the background ΔV_{lens} is assumed to be uncertain between 0% and 20% (0–400 m/s).

When the velocity model is laterally inhomogeneous, the migration velocity depends on the midpoint and the offset. We use straight-ray approximations with a variable velocity along the path to calculate the demigration velocity for each model point ℓ_m.

As in the previous examples, we show the results of uncertainty analysis of the absolute depths of the migrated reflectors and the relative depth of the deeper reflector with respect to the shallower one. We see from Figure 7 that the uncertainty in the depth of the reconstructed reflectors is laterally varying. The uncertainty is much larger in the middle of the model than at the edges due to the effect of the random fast lens.

Our results show that when the velocity model used for migration is completely wrong, then, not surprisingly, the depths of the imaged horizons will be wrong, too. In addition, we are able to make more detailed observations such as that the true horizon positions are not inside the error bars calculated using incorrect assumptions, as expected, because the true velocity is not contained in our family of admissible velocity models. However, if the velocity uncertainty is constrained to the overburden, then the relative depths may be recovered more accurately. This example shows that migrated images may contain information that is unreliable (in this case, absolute depths), and other information that is more reliable (in this case, relative depths). By performing careful analysis, we explicitly identify which quantities derived from the image we can trust and which we cannot.

Our conclusions about the quality of reconstruction of absolute versus relative depths are specific to the chosen model and the assumptions made about the velocity uncertainty. Different assumptions would lead to completely different analysis results and hence different interpretations. Here, we advocate a general framework for calculating uncertainty in various quantities of interest derived from migrated images. Proper analysis will not always lead to a reduced uncertainty, but it will lead to the correct estimate of the uncertainty.

DISCUSSION

The results presented here show that uncertainty estimates for seismic images can be generated in a theoretically sound way. The numerical examples presented here are simple. This is by design, to illustrate a methodology that allows for the quantification of uncertainty in seismic imaging. The underlying theory extends directly to more complicated models. The key to generalizing this work lies in the replacing of manually picked events with some sort of automatic data decomposition, as mentioned above; along with that extension it will be necessary to improve the computational efficiency of the method so that a sufficient number of sample data sets can be generated. Such research is already underway in the context of full-waveform inversion (Virieux and Operto, 2009; Käufl et al., 2013), and much of that work could be applied to the problems studied here. Calculating posteriors for more realistic velocity perturbation models will be computationally difficult. Smart sampling strategies when computing statistical distributions are essential.

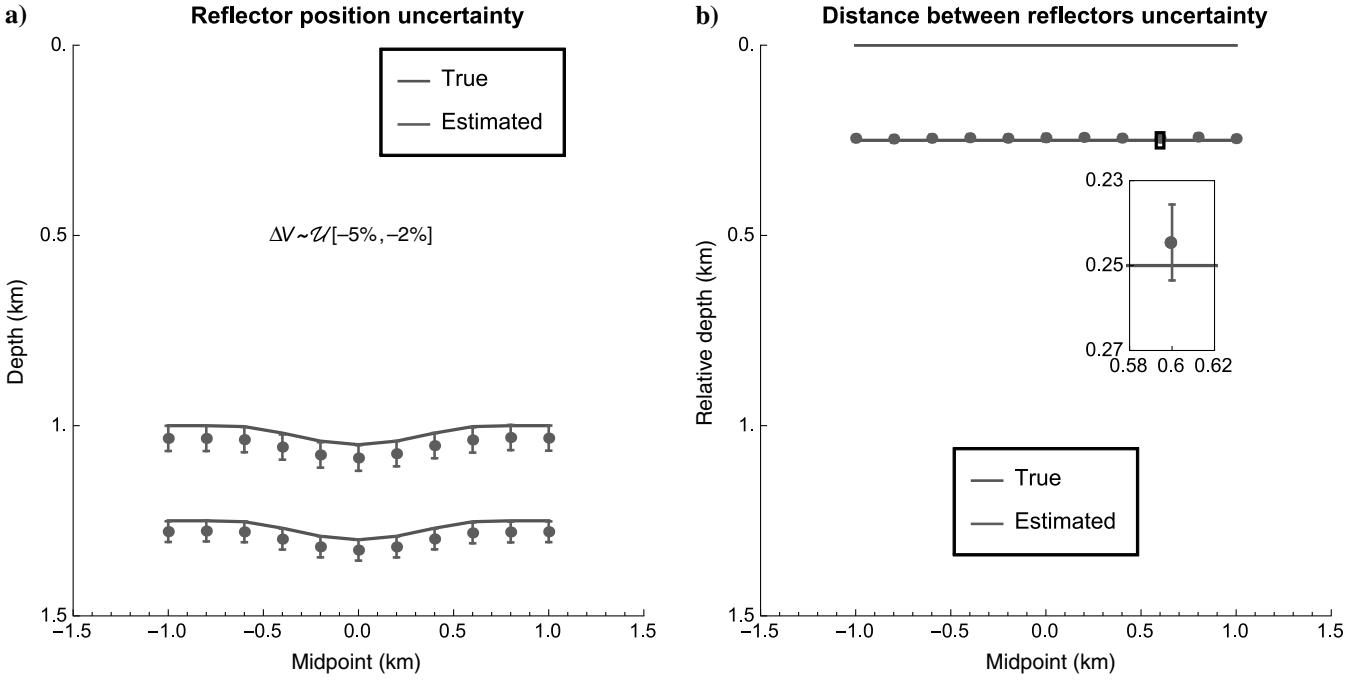

Figure 5. (a and b) Same as Figure 3 but with $\Delta V \sim \mathcal{U}[-5\%, -2\%]$. Note that now the true locations are no longer included in the error bars because the true velocity is not included in the admissible set of velocity models.

Downloaded 01/12/16 to 18.51.1.3. Redistribution subject to SEG license or copyright; see Terms of Use at http://library.seg.org/

The observation that the relative positions of reflectors can have smaller uncertainties than their absolute positions is of key importance. This is likely to hold with whatever method is used to form the image and is physically reasonable because much of the path the data follow is shared. We have theoretically explained why this is the case, and we have shown that the reduction in uncertainty can be significant. The applications of this include the estimation of the depth of subsequent reflectors once a single reflection has been identified during drilling, improved confidence in reservoir thickness estimates, and in the alleviation of statics problems.

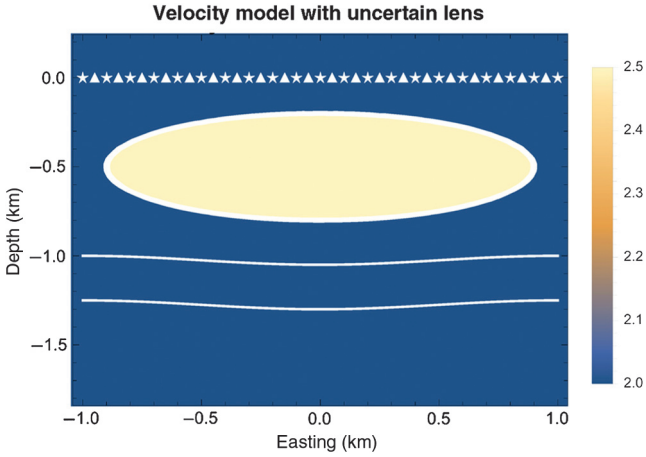

Figure 6. A numerical acoustic model with a background velocity 2 km/s, two reflectors, and sources and receivers at the surface. A fast lens is included above the reflectors. The velocity inside the lens is constant with values chosen at random from 2 to 2.5 km/s ($\Delta V_{\text{lens}} \sim \mathcal{U}[0\%, 20\%]$).

CONCLUSIONS

Seismic migration inherently relies on an available velocity model. However, a good velocity model may not be available, and even the best velocity analysis will yield a set of plausible velocity models rather than a single model. The resulting migrated image should incorporate the uncertainty of the parameters used to build the image. We have proposed a Bayesian framework to quantify uncertainty in the migrated images. We considered the effect of velocity uncertainty and the effect of the picking error. Prior information about the velocity model and assumptions about picking allowed us to construct a posterior estimate of the locations of the migrated events. This estimate not only produced a single location for each event, but it also captured the uncertainty in those locations. In some geometries, such as surface seismic and structures with relatively small deviations from horizontal, raypaths from sources and receivers to different structures largely overlap. This allows for the possibility of shared-path cancellation for velocity models with large-scale perturbations in which most of the traveltime errors are induced by a large uncertain overburden. The effect of the velocity uncertainty along the shared path is reduced, which results in better imaging of one structure relative to another.

ACKNOWLEDGMENTS

We would like to acknowledge Total for their support, and we thank P. Williamson of Total for thorough discussions of this

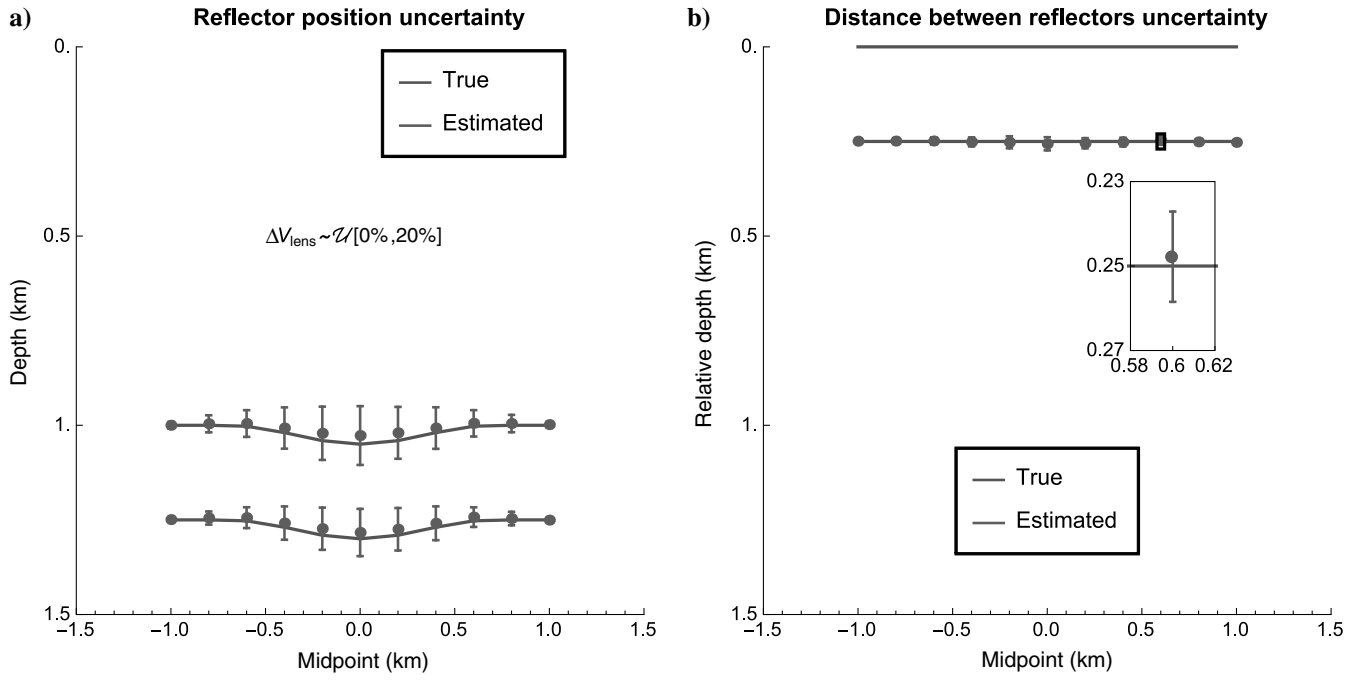

Figure 7. (a) Variations in the position of the migrated reflectors for the model shown in Figure 6. (b) The relative depth of the second reflector with respect to the depth of the first one. The introduction of the lens results in a change in error bars that change with midpoint, but the overall conclusion that the relative depth is more accurately recovered remains unchanged.

project. We would also like to acknowledge the useful interactions with M. Willis of Halliburton and B. Rodi of MIT.

REFERENCES

Bube, K. P., J. A. Kane, T. Nemeth, D. Medwedeff, and O. Mikhailov, 2004a, The influence of stacking velocity uncertainties on structural uncertainties: 74th Annual International Meeting, SEG, Expanded Abstracts, 2188–2191.

Bube, K. P., T. Nemeth, O. Mikhailov, D. Medwedeff, and J. A. Kane, 2004b, The influence of uncertainties in anisotropy on structural uncertainties: 74th Annual International Meeting, SEG, Expanded Abstracts, 2192–2195.

Douma, H., and M. V. de Hoop, 2006, Explicit expressions for prestack map time-migration in isotropic and VTI media and the applicability of map depth-migration in heterogeneous anisotropic media: Geophysics, **71**, no. 1, S13–S28, doi: 10.1190/1.2159057.

Douma, H., and M. V. de Hoop, 2007, Leading-order seismic imaging using curvelets: Geophysics, **72**, no. 6, S231–S248, doi: 10.1190/1.2785047.

Fomel, S., and E. Landa, 2014, Structural uncertainty of time-migrated seismic images: Journal of Applied Geophysics, **101**, 27–30, doi: 10.1016/j.jappgeo.2013.11.010.

Glogovsky, V., E. Landa, S. Langman, and T. J. Moser, 2009, Validating the velocity model: The Hamburg score: First Break, **27**, 77–85.

Grubb, H., A. Tura, and C. Hanitzsch, 2001, Estimating and interpreting velocity uncertainty in migrated images and AVO attributes: Geophysics, **66**, 1208–1216, doi: 10.1190/1.1487067.

Kane, J. A., W. Rodi, K. P. Bube, T. Nemeth, O. Mikhailov, and D. Medwedeff, 2004, Structural uncertainty and Bayesian inversion: 74th Annual International Meeting, SEG, Expanded Abstracts, 1511–1514.

Käufl, P., A. Fichtner, and H. Igel, 2013, Probabilistic full waveform inversion based on tectonic regionalization-development and application to the Australian upper mantle: Geophysical Journal International, **193**, 437–451, doi: 10.1093/gji/ggs131.

Osypov, K., M. O'Briain, P. Whitfield, D. Nichols, A. Douillard, P. Sexton, and P. Jouslin, 2011, Quantifying structural uncertainty in anisotropic model building and depth imaging: Hild case study: 76th Annual International Conference and Exhibition, EAGE, Extended Abstracts, F010.

Poliannikov, O. V., M. Prange, A. E. Malcolm, and H. Djikpesse, 2013, A unified Bayesian framework for relative microseismic location: Geophysical Journal International, **194**, 557–571, doi: 10.1093/gji/ggt119.

Poliannikov, O. V., M. Prange, A. E. Malcolm, and H. Djikpesse, 2014, Joint location of microseismic events in the presence of velocity uncertainty: Geophysics, **79**, no. 6, KS51–KS60, doi: 10.1190/geo2013-0390.1.

Pon, S., and L. R. Lines, 2005, Sensitivity analysis of seismic depth migrations: Geophysics, **70**, no. 2, S39–S42, doi: 10.1190/1.1897036.

Tierney, L., 1994, Markov chains for exploring posterior distributions: The Annals of Statistics, **22**, 1701–1728.

Virieux, J., and S. Operto, 2009, An overview of full-waveform inversion in exploration geophysics: Geophysics, **74**, no. 6, WCC1–WCC26, doi: 10.1190/1.3238367.

Yilmaz, O., 2001, Seismic data analysis: Processing, inversion, and interpretation of seismic data, 2nd ed.: SEG.

Downloaded 01/12/16 to 18.51.1.3. Redistribution subject to SEG license or copyright; see Terms of Use at http://library.seg.org/